International Journal of Advances in Engineering and Management (IJAEM)
Volume 4, Issue 11 Nov. 2022, pp: 01-13 www.ijaem.net ISSN: 2395-5252

Investigation of thermo-hydromagnetic stabilization of Cu-Ga and Cu/Diamond-Ga nanofluid regarding Cu-water in a porous media

Pius Erheyovwe Bubu*[1]. Chigozie Israel-Cookey[2],Valentine Benjamin Omubo-Pepple[3],Friday Barikpe Sigalo[4]

*1. Ph.D student, Department of Physics, Faculty of Science, Rivers State University, Port Harcourt, Nigeria,
2,3,4. Professor, Department of Physics, Faculty of Science, Rivers State University, Port Harcourt, Nigeria,*

Submitted: 25-10-2022 Accepted: 04-11-2022

ABSTRACT: Numerical experiments of thermo-hydromagnetic stabilization of liquid-metal based nanofluid consisting of Gallium liquid metal as base fluid with copper nanoparticles and then Cu/Diamond mixed nanoparticles in a Darcy and Darcy-Brinkman porous media is performed with the Chebyshev spectral technique for the resolution of the eigenvalue problem derived from the stability analysis of the system. The effects of the modified magnetic Chandrasekhar number Q, Nanoparticle Rayleigh number R_N, modified diffusivity ratio N_A, modified specific heat increment N_B, Lewis number Le, Darcy number D_aFurthermore, porosity ε on stabilization concerning critical Rayleigh numbers of the respective nanofluidic system are presented graphically and tabularly for the respective nanofluidic system and are compared. There is an excellent agreement between the results obtained from the numeric experiments and available results in the literature reviewed.**KEYWORDS:(11 Bold)**Mixed nanoparticles, Liquid-metal Nanofluid, Critical Rayleigh number, Chebyshev spectral method, porous media, Brownian motion and Thermophoresis.

I. INTRODUCTION

Very shortly, most industrial device and machinery cooling systems will be filled with base liquid-metal nanofluids as coolants. Qureshi et al. (2016) describe Nanofluids as a novel dynamic sub-class of nanotechnology. Nanofluid or nano-liquid is commonly the result of mixing nanoparticles with a base fluid. The base fluid recently and most investigated is water, but other fluids can be synthesized, such as liquid metal modelled in the system under investigation in this research work. These concepts of liquid metals as the base fluid for nanofluids are a highly viable study area in heat transfer developments (Kun-Quan et al., 2006). The need to develop a significantly higher thermal conductive and better heat transfer fluid apart from the conventional fluids such as water, oil, and ethylene glycol as coolants resulted in comprehensive research about nanofluid's characteristics. Usual nanofluids are generally made by dispersing nanoparticles such as copper or aluminium into the conventional liquids mentioned above. (Sakshi et al, 2011; Jing et al, 2006; Chang 2014; Siddiqui et al., 2020). Nield et al. (2017) reviewed that nanofluid is a distinctive kind of multicomponent fluid. They also describe nanofluids as suspensions of particles unusually small in size within the range between 1 and 100nm suspended in a base fluid, which can also be an organic solvent. Nanofluids form very stable colloidal systems with very little settling and significant enhancement of effective thermal conductivity compared to the base fluid, as observed in some experiments. There are two different methods to study nanofluid systems: the effect of properties variation and the Buongiorno model. Arora et al. (2011) employed the effect of the variation of properties such as size and particle concentration, thermal conductivity, pressure and temperature to postulate that nanofluid is a future industrial coolant. Wakif et al. (2018) used the heterogeneous generalized Buongiorno model to investigate the onset of nanofluid convection under

International Journal of Advances in Engineering and Management (IJAEM)
Volume 4, Issue 11 Nov. 2022, pp: 01-13 www.ijaem.net ISSN: 2395-5252

the influence of a uniform transverse magnetic field. (Nield et al., 2017) also describe the Buongiorno model of the nanofluid as a two-component mixture (base fluid plus nanoparticles) with the following assumptions: Incompressible flow; No chemical reactions; Negligible external forces; Dilute mixture; Negligible viscous dissipation; Negligible radiative heat transfer; Nanoparticles and base fluid locally in thermal equilibrium. Hence, the formulation of conservation equations applicable to the liquid-metal-based nanofluid under investigation in the absence of a solid matrix is first outlined in the next section of this investigation.

However, the key objective of this study is to investigate the stability and flow of Cu-Ga, Cu/Diamond-Ga and then compare it with that of Cu-Water nanofluid by numerically observing the effects of Da, Le, Pr, Rn on critical stability parameters under the influence of vertical magnetic field in a porous media.

II. CONSTRUCTION OF THE NANOFLUIDIC SYSTEM(11 BOLD)

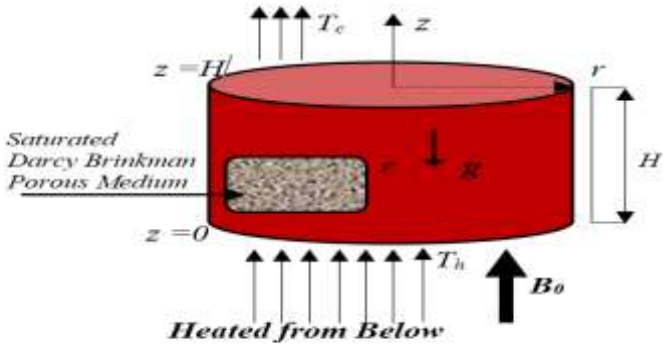

Figure 1. The Physical Geometry of the Problem

The geometry of the problem modelled is shown above in Figure 1, and the incompressible nano-liquid-metal is confined in a non-circular, very short vertical cylindrical enclosure saturated within Darcy-Brinkman porous medium heated uniformly from below with high temperature, T_h, and cooled from above at T_c is considered. The system is, however, subjected to both gravitational field $\vec{g}_{=}(0,0,g)$ and a uniform vertical upward external magnetic field $\vec{B}_{=}(0,0,B_0)$. The non-circular vertical sidewalls of the systems are adiabatic. ϕ_h and ϕ_c are taken as the corresponding volume fractions of the nanoparticles at the lower and upper regions of the nanofluidic system. A top-heavy and bottom-heavy distribution is set up for the nano-liquid-metal model, as shown in Figure 1 above. Vertical impermeable no-slip boundary walls like Niel et al. (2017), and the Rigid-Rigid case are adopted for perfectly heat conducting but electrically non-conductive.

A two-dimensional, steady, laminar and again incompressible magneto nanofluid flow and heat transfer are herein considered within the modelled confinement. The following thermophysical properties of the nanofluid system such as viscosity, thermal conductivity, specific heat, magnetic permeability and electrical conductivity are assumed to be constant, particularly in the neighbourhood of the lower temperature T of the upper region of the system except for the momentum equations which is based on the Oberbeck-Boussinesq approximations. The nanoparticles and the liquid metals are in thermal equilibrium locally; viscous dissipation and radiative heat transfer are negligible; the mixture is diluted; the reactions are non-chemical and laminar flow occurs at the onset of convection. The dimensionless conservation equation of continuity, momentum, energy, as well as nanoparticles volume fraction and modified maxwell equations are formed from the dimension equations (2.1) to (2.6) and presented below as follows:

International Journal of Advances in Engineering and Management (IJAEM)
Volume 4, Issue 11 Nov. 2022, pp: 01-13 www.ijaem.net ISSN: 2395-5252

$$\vec{\nabla}^*.\vec{u}^* = \frac{\partial \vec{u}_r^*}{\partial r^*} + \frac{\vec{u}_r^*}{r^*} + \frac{1}{r^*}\frac{\partial \vec{u}_\varphi^*}{\partial \varphi^*} + \frac{\partial \vec{u}_z^*}{\partial z^*} = 0 \quad (1)$$

$$\frac{\rho_{lm}}{\varepsilon}\frac{\partial \vec{u}_r^*}{\partial t^*} + \frac{\rho_{lm}}{\varepsilon^2}\left(\vec{u}_r^*\frac{\partial \vec{u}_r^*}{\partial r^*} + \vec{u}_z^*\frac{\partial \vec{u}_r^*}{\partial z^*}\right) = -\frac{\partial p^*}{\partial r^*} + \tilde{\mu}_{lm}\left[\frac{\partial^2 \vec{u}_r^*}{\partial r^{*2}} + \frac{1}{r^*}\frac{\partial \vec{u}_r^*}{\partial r^*} + \frac{\partial^2 \vec{u}_r^*}{\partial z^{*2}}\right] - \frac{\mu_{lm}}{k}\vec{u}_r^* + \rho\vec{g}_r + \frac{\mu_e}{4\pi}\left(\vec{\nabla}^* \times \vec{B}^*\right)\vec{B}^* \quad (2)$$

$$\frac{\rho_{lm}}{\varepsilon}\frac{\partial \vec{u}_z^*}{\partial t^*} + \frac{\rho_{lm}}{\varepsilon^2}\left(\vec{u}_r^*\frac{\partial \vec{u}_z^*}{\partial r^*} + \vec{u}_z^*\frac{\partial \vec{u}_z^*}{\partial z^*}\right) = -\frac{\partial p^*}{\partial z^*} + R_M + \tilde{\mu}_{lm}\left[\frac{\partial^2 \vec{u}_z^*}{\partial r^{*2}} + \frac{1}{r^*}\frac{\partial \vec{u}_z^*}{\partial r^*} + \frac{\partial^2 \vec{u}_z^*}{\partial z^{*2}}\right] - \frac{\mu_{lm}}{k}\vec{u}_z^* + \rho\vec{g}_z + \frac{\mu_e}{4\pi}\left(\vec{\nabla}^* \times \vec{B}^*\right) \times \vec{B}^* \quad (3)$$

$$(\rho c)_m \frac{\partial}{\partial t^*}\vec{T}^* + (\rho c)_{lm}\left(\vec{u}^*.\vec{\nabla}^*\right)\vec{T}^* = k_m\vec{\nabla}^{*2}\vec{T}^* + \varepsilon(\rho c)_p D_B\vec{\nabla}^*\phi^*.\vec{\nabla}^*T^* + \varepsilon(\rho c)_p\left(\frac{D_T}{T_c}\right)\vec{\nabla}^*T^*.\vec{\nabla}^*T^* \quad (4)$$

$$\frac{\partial}{\partial t^*}\phi^* + \frac{1}{\varepsilon}\left(\vec{u}^*.\vec{\nabla}^*\right)\phi^* = D_B\vec{\nabla}^{*2}\phi^* + \frac{D_T}{T_c}\vec{\nabla}^{*2}\vec{T}^* \quad (5)$$

$$\vec{\nabla}.\vec{B} = \frac{\partial \vec{B}_r}{\partial r} + \frac{\varrho\vec{B}_r}{r} + \frac{\partial \vec{B}_z}{\partial z} = \frac{\varrho}{r}\frac{\partial(r\vec{B}_r)}{\partial r} + \frac{\partial \vec{B}_z}{\partial z} = 0 \quad (6)$$

The above equations are transformed to dimensionless using the following non-dimensionless dependent and independent variables: $(r, z) \to \left(\frac{r^*}{h}, \frac{z^*}{h}\right)$, $\vec{u} \to (\vec{u}_r, \vec{u}_z) \to (\vec{u}_r^*, \vec{u}_z^*)\frac{(\rho c)_{lm}\, h}{k_m}$, $h\nabla \to \nabla^*$, $t \to \frac{k_m}{(\rho c)_{lm}\, h^2}t^*$, $T \to \frac{(T^* - T_c)}{(T_h - T_c)}$, $\phi \to \frac{(\phi^* - \phi_h)}{(\phi_c - \phi_h)}$, $\vec{B} \to \left(\frac{1}{\vec{B}_0}\right)\vec{B}^*$; and these magneto nanofluids are characterized by the following dimensionless parameters: D_a= Darcy number, is dimensionless permeability= $\frac{\tilde{\mu}k}{\mu H^2}$, R_a = Thermal Rayleigh Number = $\frac{\rho_0 gkH\,\beta}{(\mu\alpha_m)}(T_h - T_c)$, R_M = Density Rayleigh Number = $\frac{gkH}{\mu\alpha_m}\left[\phi_h\rho_p + \rho_0(1 - \phi_h)\right]$, R_N = Nanoparticle Rayleigh Number = $\frac{gkH}{\mu\alpha_m}(\phi_c - \phi_h)(\rho_p - \rho_0)$, P_r = Prandtl number = $\frac{\mu}{\rho_0\alpha_m}$, P_{rM} = the magnetic Prandtl number = $\frac{\mu}{\rho_0\eta}$, $\mathbf{V_a}$ = Vadasz Number = $\frac{\varepsilon H^2 P_r}{k} = \frac{\varepsilon P_r}{D_a}$ Q = the modified magnetic Chandrasekhar number = $\frac{\mu_e k}{(4\pi\varepsilon\mu\eta)}B_0^2$, N_A = $\frac{D_T}{T_h D_B \phi_0}(T_h - T_c)$ the modified diffusivity ratios, Le = Lewis number = $\frac{\alpha_m}{(\varepsilon D_B)}$ and N_B = modified particle-density increment = $\frac{\varepsilon(\rho c)_p \phi_0}{(\rho c)_{lm}}$, $\delta = \frac{(\rho c)_m}{(\rho c)_{lm}}$ is the ratio of nanofluid's effective heat capacity to liquid metal's heat capacity and the MHD-nanofluidic thermo-physical parameters.

The corresponding boundary conditions are associated with the dimensionless conservation equations:

$$\vec{u}_z = \frac{\partial \vec{u}_z}{\partial z} = 0;\ T = 0;\ \phi = 1;\ \vec{B} = \vec{e}_z;\ \vec{\nabla} \times \vec{B} = 0;\ \frac{d\phi_{bs}}{dz} + N_A\frac{dT_{bs}}{dz} = 0 \text{ at } z = 0 \quad (7)$$

$$\vec{u}_z = \frac{\partial \vec{u}_z}{\partial z} = 0;\ T = 0;\ \phi = 1;\ \vec{B} = \vec{e}_z;\ \vec{\nabla} \times \vec{B} = 0;\ \frac{d\phi_{bs}}{dz} + N_A\frac{dT_{bs}}{dz} = 0 \text{ at } z = 1$$

III. STABILITY ANALYSIS OF THE SYSTEM (11 BOLD)

The basic state of the nanofluidic system can analytically be described as follows:

$$\vec{u}_{xbs} = \vec{u}_{zbs} = 0;\ \vec{B} = \vec{B}_{bs}e_Z;\ T_{bs} = T_{bs}(z);\ P_{bs} = P_{bs}(z);\ \phi_{bs} = \phi_{bs}(z). \quad (7)$$

The basic steady state for equations (7) to (12) is denoted by subscript "bs". In the analytic investigation, the time-independence solution only seeks temperature, nanoparticle volume fraction, and magnetic inductance in the z-direction. Then, Equations (1) – (6) therefore reduces to:

$$\frac{\partial P_{bs}}{\partial z} = R_M + (R_a T - R_N\phi)e_z + \frac{\varepsilon P_r Q\vec{B}_0^2}{P_{rM}} \quad (8)$$

$$\frac{d^2T_{bs}}{dz^2} + \frac{N_B}{L_e}\left(\frac{d\phi_{bs}}{dz}\right)\left(\frac{dT_{bs}}{dz}\right) + \frac{N_A N_B}{L_e}\left(\frac{dT_{bs}}{dz}\right)^2 = 0 \quad (9)$$

$$\left(\frac{d^2\phi_{bs}}{dz^2}\right) + N_A\left(\frac{d^2T_{bs}}{dz^2}\right) = 0 \quad (10)$$

$$\frac{d\vec{B}_z}{dz} = 0 \quad (11)$$

The basic solutions $T_{bs}(z) = 1 - z$ and $\phi_{bs}(z) = z$ linear copper nanoparticles in z are in the spirit of (Yadav et al., 2013).

International Journal of Advances in Engineering and Management (IJAEM)
Volume 4, Issue 11 Nov. 2022, pp: 01-13 www.ijaem.net ISSN: 2395-5252

Linear Perturbation Equations:

The basic solution state can be superimposed with infinitesimal perturbations fields, such that: $\vec{B} = \vec{B}_{bs}(z) + \vec{B}'$; $\vec{u} = \vec{u}_{bs}(z) + \vec{u}'$; $T = T_{bs}(z) + T'$; $\phi = \phi_{bs}(z) + \phi'$; and $P = P_{bs}(z) + P'$ (12)

$\vec{B}'$, $\vec{u}'$, T', ϕ', and P' are the perturbed quantities over their respective equilibrium counterparts are functions of r, z, and t. Equations (2.1) to (2.6) are linearized by neglecting products of the primed quantities concerning the perturbations as well as taking $\vec{u}_{bs} = 0$ and $\vec{B}_{bs} = \vec{e}_z$ gives

$$\vec{\nabla}.\vec{u}' = \frac{\partial \vec{u}_z'}{\partial z} = 0 \quad (13)$$

$$\frac{1}{V_a}\left(\frac{1}{\delta}\frac{\partial \vec{u}_z'}{\partial t}\right) = -\frac{\partial P}{\partial z} + R_M + D_a\left(\frac{\partial^2 \vec{u}_z'}{\partial z^2}\right) - \vec{u}_z' + (R_a T - R_N \phi)e_z + \frac{\varepsilon P_r Q}{P_{rM}}\frac{\partial \vec{B}'}{\partial z} \quad (14)$$

$$\frac{\partial T'}{\partial t} + \left(\vec{u}_z'\frac{\partial T_{bs}}{\partial z}\right) = \left(\frac{\partial^2 T'}{\partial z^2}\right) + \frac{N_B}{L_e}\left(\frac{\partial T'}{\partial z} - \frac{\partial \phi'}{\partial z}\right) - \frac{2N_A N_B}{L_e}\frac{\partial T'}{\partial z} \quad (15)$$

$$\frac{\varepsilon}{\delta}\frac{\partial \phi'}{\partial t} + u_z'\frac{\partial \phi'}{\partial z} = \frac{1}{L_e}\left(\frac{\partial^2 \phi'}{\partial z^2}\right) + \frac{N_A}{L_e}\left(\frac{\partial^2 T'}{\partial z^2}\right) \quad (16)$$

$$\frac{\varepsilon}{\delta}\frac{\partial \vec{B}'}{\partial t} = \frac{\partial u_z'}{\partial z} + \frac{\varepsilon P_r}{P_{rM}}\left(\frac{\partial^2 \vec{B}'}{\partial z^2}\right) \quad (17)$$

$$\vec{\nabla}.\vec{B}' = 0 \quad (18)$$

Performing Operation on Eq. (14) twice with curl operator, $\vec{e}_z.curlcurl$ and the identity, $curlcurl \equiv grad\ div - \nabla^2$, as well as using Eq. (13) and taking again only the z component of the resulting momentum and Maxwell's equation, the pressure term P' is eliminated from the momentum Equation (3.48). Therefore, reducing the unknowns to $\vec{B}'$, $\vec{u}'$, T', and ϕ' according to:

$$\frac{1}{V_a}\left(\frac{1}{\delta}\frac{\partial \vec{\nabla}^2 \vec{u}_z'}{\partial t}\right) = \left(D_a\frac{\partial^2}{\partial z^2} - 1\right)\vec{\nabla}^2\vec{u}_z' + R_a\vec{\nabla}_2^2 T' - R_N\vec{\nabla}_2^2\phi' + Q\frac{\partial}{\partial z}\left(\frac{\varepsilon P_r}{P_{rM}}\frac{\partial^2 \vec{B}'}{\partial z^2}\right) \quad (19)$$

The perturbation quantities are assumed to be of the form:

$$(\psi', T', C', B_z') = [\psi(z), \theta(z), C(z), B(z)]\ e^{\lambda_n t} J_n(ar)cos(n\varphi) \quad (20)$$

By substituting equation (20) into the resulting equations (16) to (19), the linearized equations still in the dimensionless form are obtained as follows:

$$\frac{\lambda_n}{\delta V_a}(D_n^2 - \alpha^2)\alpha\psi = \alpha\left[D_a\left((D_n^2 - \alpha^2) - 1\right)\right](D_n^2 - \alpha^2)\psi - R_a\alpha^2\theta + R_N\alpha^2 C + QD_n\left(\frac{\varepsilon\lambda_n}{\delta}B + \alpha D_n\psi\right) \quad (21)$$

$$\lambda_n\theta + \alpha\psi = (D_n^2 - \alpha^2)\theta + \frac{(1-2N_A)N_B}{L_e}D_n\theta + \frac{N_B}{L_e}D_n C \quad (22)$$

$$\frac{\varepsilon}{\delta}\lambda_n C - \alpha\psi = \frac{1}{L_e}(D_n^2 - \alpha^2)C + \frac{N_A}{L_e}(D_n^2 - \alpha^2)\theta \quad (23)$$

$$\frac{\varepsilon}{\delta}\lambda_n B + \alpha D\psi = \frac{\varepsilon P_r}{P_{rM}}(D_n^2 - \alpha^2)B \quad (24)$$

In equations (21) to (24) $D_n = \frac{\partial}{\partial z}.D\psi = \psi = \theta = C = D_n B = 0$ at $z = 0{,}1$ for normal mode analysis is the first boundary condition for the above equation. The equation is an eigenvalue problem expression which is the same algebraically in form as found by (Wakif et al., 2017; Wakif et al., 2016; Barletta et al. 2013) studied a very short porous channel. This radially symmetric porous cylindrical media with aspect ratio A is endowed with a discrete spectrum. The principle of exchange of stability is assumedly valid for this investigation. For the investigation of stationary mode, the growth rate λ_n for each disturbance, $\lambda_n = 0$, consequently the equations (21) to (24) becomes

$$[-D_a D_n^4 + (2\alpha^2 D_a + Q + 1)D_n^2 - \alpha^2(D_a\alpha^2 + 1)]\psi + R_N\alpha C = R_a\alpha\theta \quad (25)$$

$$\alpha\psi - \left(D_n^2 + \frac{(1-2N_A)N_B}{L_e}D_n - \alpha^2\right)\theta + \frac{N_B}{L_e}D_n C = 0 \quad (26)$$

$$\alpha\psi + \frac{1}{L_e}(D_n^2 - \alpha^2)C + \frac{N_A}{L_e}(D_n^2 - \alpha^2)\theta = 0 \quad (27)$$

The simplified system of equations (25), (26), and (27) are solved within the following boundary conditions:

$$D\psi = \psi = \theta = C = D_n B = 0 \text{ at } z = 0{,}1. \quad (28)$$

International Journal of Advances in Engineering and Management (IJAEM)
Volume 4, Issue 11 Nov. 2022, pp: 01-13 www.ijaem.net ISSN: 2395-5252

Computational Procedure:

The eigenvalue equations obtained above are solved numerically for the rigid-rigid magneto nanofluid boundaries case for different values of N_A, N_B, R_N, Le, Da, Q using the Chebyshev-Tau spectral method to find the critical Rayleigh number R_{ac} as a function of critical wave number a_c. To solve the normal mode model by the Chebyshev-Tau method together with the boundary conditions

$$Az = \sigma Bz \quad (29)$$

$$\begin{pmatrix} A_{11}A_{12}A_{13} \\ A_{21}A_{22}A_{23} \\ A_{31}A_{32}A_{33} \end{pmatrix} \begin{pmatrix} \psi \\ \theta \\ C \end{pmatrix} = R_a \begin{pmatrix} B_{11}B_{12}B_{13} \\ B_{21}B_{22}B_{23} \\ B_{31}B_{32}B_{33} \end{pmatrix} \begin{pmatrix} \psi \\ \theta \\ C \end{pmatrix} \quad (30)$$

The system of equations (2.25), (2.26), and (2.27) is an eigenvalue problem of R_a, for fixed. Let R_{ac} be the least positive eigenvalue of the system where Linear stability occurs if $R_a < R_{ac}$ and linear instability if $R_a > R_{ac}$. We therefore have

$$[-D_a D_n^4 + (2\alpha^2 D_a + Q + 1)D_n^2 - \alpha^2(D_a\alpha^2 + 1)]\psi + R_N \alpha C = R_a \alpha\theta \quad (a)$$

$$\alpha\psi - \left(D_n^2 + \frac{(1-2N_A)N_B}{L_e} D_n - \alpha^2\right)\theta + \frac{N_B}{L_e} D_n C = 0 \quad (b)$$

$$\alpha\psi + \frac{N_A}{L_e}(D_n^2 - \alpha^2)\theta + \frac{1}{L_e}(D_n^2 - \alpha^2)C = 0 \quad (c)$$

(31a-c)

The conditions at $z = -1,1$ are known as clamped boundary conditions. The D^2 Chebyshev-tau method is applied to resolve the eigenvalue problem by writing the system of equations thus:

$$L_1(\psi, C, \theta)^T = [-D_a D_n^4 + (2\alpha^2 D_a + Q + 1)D_n^2 - \alpha^2(D_a\alpha^2 + 1)]\psi + R_N \alpha C - R_a \alpha\theta = 0 \quad (a)$$

$$L_2(\psi, C, \theta)^T = \alpha\psi - \left(D_n^2 + \frac{(1-2N_A)N_B}{L_e} D_n - \alpha^2\right)\theta + \frac{N_B}{L_e} D_n C = 0 \quad (b)$$

$$L_3(\psi, C, \theta)^T = \alpha\psi + \frac{1}{L_e}(D_n^2 - \alpha^2)C + \frac{N_A}{L_e}(D_n^2 - \alpha^2)\theta = 0 \quad (c)$$

(32a-c)

The system (3.31) is transformed from (0,1), the natural domain, into the spatial domain $(-1,1)$ as finite truncated series of Chebyshev polynomials:

$$\psi = \sum_{i=0}^{N+2} \psi_i T_i(z) \quad (a)$$

$$C = \sum_{i=0}^{N+2} c_i T_i(z) \quad (b)$$

$$\theta = \sum_{i=0}^{N+2} \theta_i T_i(z) \quad (c)$$

(33a-c)

Meanwhile, the exact solution to (3.78) is an infinite series, $N \to \infty$.

$$\psi_i = c_i = \theta_i = cos(icos^{-1}(z)),\ i = 1,2,3 \ldots . \quad (34)$$

The Chebyshev tau assertion of equation (34) is solved with the approximate form (35) because of the truncation by using

$$L_1(\psi, C, \theta)^T = \tau_{11} T_{N+1} + \tau_{12} T_{N+2} \quad (a)$$

$$L_2(\psi, C, \theta)^T = \tau_{21} T_{N+1} + \tau_{22} T_{N+2} \quad (b)$$

$$L_3(\psi, C, \theta)^T = \tau_{31} T_{N+1} + \tau_{32} T_{N+2} \quad (c)$$

(35a-c)

In (35) above, the parameters $\tau_{11}, \ldots, \tau_{32}$ are the tau coefficients while L_1, L_1, L_3 are the differential operator. According to Lanczos's technic and Fox error analysis, the tau coefficient parameters are effectively used to measure or indicate the error associated with truncation in (34). (Straughan et al., 1996)

The Chebyshev scheme above is applied to the system of equations (30), and (31) to solving (29) were now

$$z = (\psi_o, \ldots, \psi_{N+2}, c_o, \ldots, c_{N+2}, \theta_o, \ldots, \theta_{N+2})^T \quad (36)$$

And the matrices A and B are given by

$$A = \begin{pmatrix} -D_a D_n^4 + (2\alpha^2 I D_a + Q + 1)D_n^2 - \alpha^2 I(D_a\alpha^2 + 1) & 0 & R_N \alpha I \\ \alpha I & -\left(D_n^2 + \frac{(1-2N_A)N_B}{L_e} D_n - \alpha^2 I\right) & \frac{N_B}{L_e} D_n \\ \alpha I & \frac{N_A}{L_e}(D_n^2 - \alpha^2 I) & \frac{1}{L_e}(D_n^2 - \alpha^2 I) \end{pmatrix} \quad (37)$$

International Journal of Advances in Engineering and Management (IJAEM)
Volume 4, Issue 11 Nov. 2022, pp: 01-13 www.ijaem.net ISSN: 2395-5252

$$B = \begin{pmatrix} 0 & aI & 0 \\ 0 & 0 & 0 \\ 0 & 0 & 0 \end{pmatrix} \quad (38)$$

To confirm the accuracy of the present study, first test computations are carried out for the stationary instability threshold of the magneto nanofluids for different values of N_A and Q in the case where: $\varepsilon = 0.9$, $D_a = 0.5$, $L_e = 100$, $R_N = 0.1$ and $N_A = 1$ within the rigid-rigid boundary. The critical Rayleigh number R_{ac} and the corresponding critical wavenumber a_c for different values of magnetic Chandrasekhar, number Q are obtained, and comparisons were made with present results and that given by Wakif et al. (2016) for electrically conducting nanofluids in Table 1. TAs a result, there is an excellent agreement, as shown in the graphical representation using Python seaborn pair-plot and line-plot in Figure 2. The resultant figures thus validate the accuracy of the method applied and ensure the present results' correctness.

Table 1: The numerical values of critical values of Rayleigh number and corresponding wave number obtained for the present work compared with Wakif et al. (2016) where $\epsilon = 0.9$, $N_A = 1$, $L_e = 100$, $D_a = 0.5$, $R_N = 0.1$

Rigid - Rigid case (N=55)					
N_B	Q	a_c	Present study	Wakif et al. (2016)	Relative Difference
			R_{ac}	R_{ac}	%
10^{-4}	0	3.1239	887.0990	887.0988	2.0×10^{-5}
	5	3.2672	1005.6500	1005.6524	-2.0×10^{-4}
	15	3.4935	1226.8400	1226.8423	-1.9×10^{-4}
	35	3.8167	1630.2800	1630.2779	1.3×10^{-5}
	75	4.2379	2356.3000	2356.3024	-1.0×10^{-5}
	100	4.4285	2779.3800	2779.3810	-4.0×10^{-5}
10^{-3}	0	3.1239	887.0990	887.0988	2.0×10^{-5}
	5	3.2672	1005.6500	1005.6524	-2.0×10^{-4}
	15	3.4935	1226.8400	1226.8423	-1.9×10^{-4}
	35	3.8167	1630.2800	1630.2779	1.3×10^{-5}
	75	4.2379	2356.3000	2356.3024	-1.0×10^{-4}
	100	4.4285	2779.3800	2779.3810	-4.0×10^{-5}
10^{-2}	0	3.1239	887.0990	887.0988	2.0×10^{-5}
	5	3.2672	1005.6500	1005.6524	-2.0×10^{-4}
	15	3.4935	1226.8400	1226.8423	-1.9×10^{-4}
	35	3.8167	1630.2800	1630.2779	1.3×10^{-4}
	75	4.2379	2356.3000	2356.3024	-1.0×10^{-5}
	100	4.4285	2779.3800	2779.3810	-4.0×10^{-5}

International Journal of Advances in Engineering and Management (IJAEM)
Volume 4, Issue 11 Nov. 2022, pp: 01-13 www.ijaem.net ISSN: 2395-5252

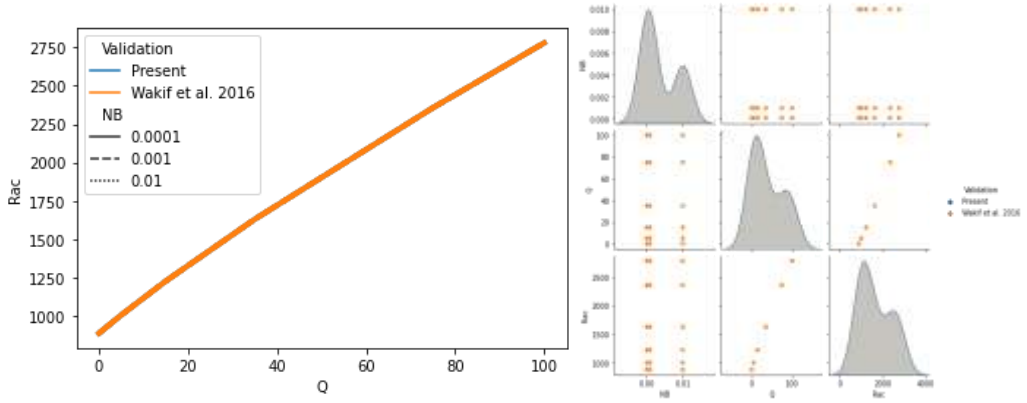

Figure 2.: A plot showing the validation of the presented results with Wakif et al. (2016) in the case of electrically conducting fluid for different values of the magnetic Chandrasekhar number Q

SOURCE CODE for THE Numerical experiments:

```
ClearAll["Global`*"];
Np=55;Da=0.5;Q=0.0;α=3.1440;Na=1.5;Nb=0.02;Le=14450.50;Rn=0.1;ϵ=0.9;

ψ=Sum[a_k * ChebyshevT[k, 2 z - 1], {k, 0, Np}];
τ=Sum[b_k * ChebyshevT[k, 2 z - 1], {k, 0, Np}];
ϕ=Sum[d_k * ChebyshevT[k, 2 z - 1], {k, 0, Np}];
B11=(ψ/.z->0)==0;
B12=(∂_z ψ/.z->0)==0;
B13=(ψ/.z->1)==0;
B14=(∂_z ψ/.z->1)==0;
B21=(τ/.z->0)==0;
B22=(τ/.z->1)==0;
B31=(ϕ/.z->0)==0;
B32=(ϕ/.z->1)==0;
B2=Join[{B11,B12,B13,B14,B21,B22,B31,B32}];

var1=Table[a_k,{k,0,3}];
var2=Table[b_k,{k,0,1}];
var3=Table[d_k,{k,0,1}];

B3=Join[{var1,var2,var3}]//Flatten;
sol1=NSolve[B2,B3]//Flatten;

ψ1=ψ/.sol1;τ1=τ/.sol1;ϕ1=ϕ/.sol1;

nodes=N[Table[(1/2*(1-Cos[(i*π)/Np])),{i,0,Np}]];

R11=Da*∂_{z,4} ψ1-(2α^2 Da+Q+1)∂_{z,2} ψ1+α^2 (1+Da*α^2)ψ1+Rn*α^2*ϕ1;
R12=ψ1+(∂_{z,2} τ1+((1-2*Na)Nb)/Le ∂_{z,1} τ1-α^2*τ1)-Nb/Le ∂_{z,1} ϕ1;
R13=ϵ-1*ψ1-Na/Le (∂_{z,2} τ1-α^2*τ1)-1/Le (∂_{z,2} ϕ1-α^2*ϕ1);
```

International Journal of Advances in Engineering and Management (IJAEM)
Volume 4, Issue 11 Nov. 2022, pp: 01-13 www.ijaem.net ISSN: 2395-5252

```
R21=Ra*α^2*τ1;
R22=0;
R23=0;

A11=Thread[(Table[R11/.z->nodes[[i]],{i,2,Np-2}])]//Flatten;
A12=Thread[(Table[R12/.z->nodes[[i]],{i,2,Np}])]//Flatten;
A13=Thread[(Table[R13/.z->nodes[[i]],{i,2,Np}])]//Flatten;
A1=Join[A11,A12,A13];
A21=Thread[(Table[R21/.Ra->1/.z->nodes[[i]],{i,2,Np-2}])]//Flatten;
A22=Thread[(Table[R22/.z->nodes[[i]],{i,2,Np}])]//Flatten;
A23=Thread[(Table[R23/.z->nodes[[i]],{i,2,Np}])]//Flatten;
A2=Join[A21,A22,A23];


var1=Table[ak,{k,4,Np}];
var2=Table[bk,{k,2,Np}];
var3=Table[dk,{k,2,Np}];
var=Join[var1,var2,var3]//Flatten;

A3=CoefficientArrays[A1,var][[2]]//Normal;
A4=CoefficientArrays[A2,var][[2]]//Normal;

Reverse[Eigenvalues[{A3,A4}]]
```

IV. OBSERVATIONS FROM THE NUMERICALABORATORY

The effects of anexternal magnetic field on the criteria of the onset of thermal convection/stabilization in Cu-Ga or Cu/Dia-Ga Nanofluid in Darcy, Darcy-Brinkman porous medium investigated for different nanoparticle distribution, top- and bottom-heavy case.The stability equation established in the numeric experiments reveals or shows how the thermal stability of the Nanofluid system depends on Q, N_B, R_N, N_A and D_A. The Lewis number serves as a distinguishing factor for the Nanofluid system, Le (Cu-Ga) is 8000, and that of Cu/Dia-Ga is14450. The variation of the critical stability parameters Rac as a function of different values of the control parameters N_B, R_N, Le, N_A or D_A are plotted graphically to visualize their effects.

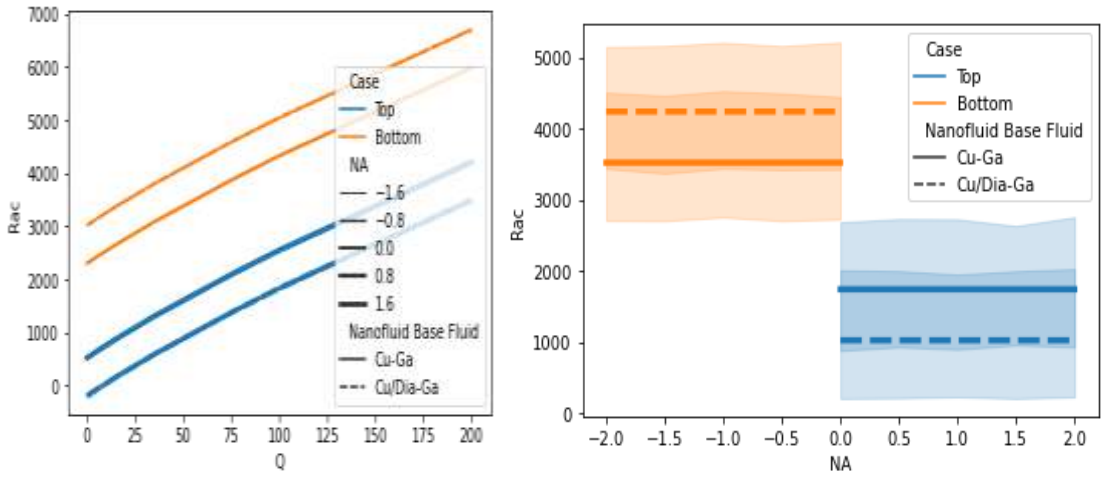

Figure 4: Results of the modified magnetic Chandrasekhar number Q effects on the critical Rayleigh number R_{ac} for different values of modified diffusivity ratio N_A for Cu-Ga and Cu/Diamond-Ga, top-heavy and bottom-heavy cases

Case	Nanofluid Base Fluid	Da	Q	Rac
Top	Cu-Ga	0.1	0	-673.91
Top	Cu-Ga	0.1	5	-569.68
Top	Cu-Ga	0.1	15	-360.37
Top	Cu-Ga	0.1	35	-8.36814
Top	Cu-Ga	0.1	75	617.74
Top	Cu-Ga	0.1	100	984.02
Top	Cu-Ga	0.1	200	2531.21
Top	Cu-Ga	0.2	0	-503.04
Top	Cu-Ga	0.2	5	-387.65
Top	Cu-Ga	0.2	15	-179.71
Top	Cu-Ga	0.2	35	189.26
Top	Cu-Ga	0.2	75	845.82
Top	Cu-Ga	0.2	100	1228.79
Top	Cu-Ga	0.2	200	2805.1
Top	Cu-Ga	0.3	0	-332.23
Top	Cu-Ga	0.3	5	-215.56
Top	Cu-Ga	0.3	15	-2.4453
Top	Cu-Ga	0.3	35	379.53
Top	Cu-Ga	0.3	75	1061.49
Top	Cu-Ga	0.3	100	1458.89
Top	Cu-Ga	0.3	200	3056.06
Top	Cu-Ga	0.4	0	-161.43
Top	Cu-Ga	0.4	5	-43.76
Top	Cu-Ga	0.4	15	173.61
Top	Cu-Ga	0.4	35	566.81
Top	Cu-Ga	0.4	75	1271.59
Top	Cu-Ga	0.4	100	1682.22
Top	Cu-Ga	0.4	200	3295.85
Top	Cu-Ga	0.5	0	9.3736
Top	Cu-Ga	0.5	5	127.93
Top	Cu-Ga	0.5	15	349.12
Top	Cu-Ga	0.5	35	752.56
Top	Cu-Ga	0.5	75	1478.53
Top	Cu-Ga	0.5	100	1901.67
Top	Cu-Ga	0.5	200	3528.9
Top	Cu/Dia-Ga	0.1	0	1149.81
Top	Cu/Dia-Ga	0.1	5	-1277.47
Top	Cu/Dia-Ga	0.1	15	-1077.16
Top	Cu/Dia-Ga	0.1	35	-725.16
Top	Cu/Dia-Ga	0.1	75	-99.05
Top	Cu/Dia-Ga	0.1	100	267.23

Top	Cu/Dia-Ga	0.1	200	1814.43
Top	Cu/Dia-Ga	0.2	0	-1219.83
Top	Cu/Dia-Ga	0.2	5	-1104.43
Top	Cu/Dia-Ga	0.2	15	-896.49
Top	Cu/Dia-Ga	0.2	35	-527.53
Top	Cu/Dia-Ga	0.2	75	129.03
Top	Cu/Dia-Ga	0.2	100	512
Top	Cu/Dia-Ga	0.2	200	2088.25
Top	Cu/Dia-Ga	0.3	0	-1049.01
Top	Cu/Dia-Ga	0.3	5	-932.34
Top	Cu/Dia-Ga	0.3	15	-719.23
Top	Cu/Dia-Ga	0.3	35	-337.26
Top	Cu/Dia-Ga	0.3	75	334.7
Top	Cu/Dia-Ga	0.3	100	742.11
Top	Cu/Dia-Ga	0.3	200	2339.27
Top	Cu/Dia-Ga	0.4	0	-878.2
Top	Cu/Dia-Ga	0.4	5	-760.54
Top	Cu/Dia-Ga	0.4	15	-543.16
Top	Cu/Dia-Ga	0.4	35	-149.97
Top	Cu/Dia-Ga	0.4	75	554.82
Top	Cu/Dia-Ga	0.4	100	965.45
Top	Cu/Dia-Ga	0.4	200	2579.07
Top	Cu/Dia-Ga	0.5	0	-707.4
Top	Cu/Dia-Ga	0.5	5	-588.85
Top	Cu/Dia-Ga	0.5	15	-367.65
Top	Cu/Dia-Ga	0.5	35	35.79
Top	Cu/Dia-Ga	0.5	75	761.82
Top	Cu/Dia-Ga	0.5	100	1184.9
Top	Cu/Dia-Ga	0.5	200	2812.1
Bottom	Cu-Ga	0.1	0	1103.87
Bottom	Cu-Ga	0.1	5	1217.1
Bottom	Cu-Ga	0.1	15	1417.41
Bottom	Cu-Ga	0.1	35	1769.41
Bottom	Cu-Ga	0.1	75	2395.51
Bottom	Cu-Ga	0.1	100	2761.8
Bottom	Cu-Ga	0.1	200	4308.96
Bottom	Cu-Ga	0.2	0	1274.73
Bottom	Cu-Ga	0.2	5	1390.13
Bottom	Cu-Ga	0.2	15	1598.07
Bottom	Cu-Ga	0.2	35	1967.64
Bottom	Cu-Ga	0.2	75	2623.6
Bottom	Cu-Ga	0.2	100	3006.58
Bottom	Cu-Ga	0.2	200	4582.88

Bottom	Cu-Ga	0.3	0	1445.56
Bottom	Cu-Ga	0.3	5	1562.22
Bottom	Cu-Ga	0.3	15	1775.33
Bottom	Cu-Ga	0.3	35	2157.3
Bottom	Cu-Ga	0.3	75	2839.26
Bottom	Cu-Ga	0.3	100	3236.67
Bottom	Cu-Ga	0.3	200	4833.83
Bottom	Cu-Ga	0.4	0	1616.36
Bottom	Cu-Ga	0.4	5	1734.03
Bottom	Cu-Ga	0.4	15	1951.4
Bottom	Cu-Ga	0.4	35	2344.59
Bottom	Cu-Ga	0.4	75	3049.38
Bottom	Cu-Ga	0.4	100	3460
Bottom	Cu-Ga	0.4	200	5073.64
Bottom	Cu-Ga	0.5	0	1787.17
Bottom	Cu-Ga	0.5	5	1905.72
Bottom	Cu-Ga	0.5	15	2126.91
Bottom	Cu-Ga	0.5	35	2530.35
Bottom	Cu-Ga	0.5	75	3256.39
Bottom	Cu-Ga	0.5	100	3679.48
Bottom	Cu-Ga	0.5	200	5306.71
Bottom	Cu/Dia-Ga	0.1	0	1820.53
Bottom	Cu/Dia-Ga	0.1	5	1933.76
Bottom	Cu/Dia-Ga	0.1	15	2134.07
Bottom	Cu/Dia-Ga	0.1	35	2486.06
Bottom	Cu/Dia-Ga	0.1	75	3112.17
Bottom	Cu/Dia-Ga	0.1	100	3478.46
Bottom	Cu/Dia-Ga	0.1	200	5025.67
Bottom	Cu/Dia-Ga	0.2	0	1991.39
Bottom	Cu/Dia-Ga	0.2	5	2106.79
Bottom	Cu/Dia-Ga	0.2	15	2314.73
Bottom	Cu/Dia-Ga	0.2	35	2683.69
Bottom	Cu/Dia-Ga	0.2	75	3340.25
Bottom	Cu/Dia-Ga	0.2	100	3723.23
Bottom	Cu/Dia-Ga	0.2	200	5299.54
Bottom	Cu/Dia-Ga	0.3	0	2162.21
Bottom	Cu/Dia-Ga	0.3	5	2278.87
Bottom	Cu/Dia-Ga	0.3	15	2491.98
Bottom	Cu/Dia-Ga	0.3	35	2873.96
Bottom	Cu/Dia-Ga	0.3	75	3555.91
Bottom	Cu/Dia-Ga	0.3	100	3953.32
Bottom	Cu/Dia-Ga	0.3	200	5550.51
Bottom	Cu/Dia-Ga	0.4	0	2332.99

International Journal of Advances in Engineering and Management (IJAEM)
Volume 4, Issue 11 Nov. 2022, pp: 01-13 www.ijaem.net ISSN: 2395-5252

Bottom	Cu/Dia-Ga	0.4	5	2450.69
Bottom	Cu/Dia-Ga	0.4	15	2668.05
Bottom	Cu/Dia-Ga	0.4	35	3061.25
Bottom	Cu/Dia-Ga	0.4	75	3766.08
Bottom	Cu/Dia-Ga	0.4	100	4176.66
Bottom	Cu/Dia-Ga	0.4	200	5790.21
Bottom	Cu/Dia-Ga	0.5	0	2503.83
Bottom	Cu/Dia-Ga	0.5	5	2622.37
Bottom	Cu/Dia-Ga	0.5	15	2843.57
Bottom	Cu/Dia-Ga	0.5	35	3246.98
Bottom	Cu/Dia-Ga	0.5	75	3973.03
Bottom	Cu/Dia-Ga	0.5	100	4396.11
Bottom	Cu/Dia-Ga	0.5	200	6023.34

V. CONCLUSION

The numerical solutions of the stabilization of magneto liquid-metal, Cu-Ga and Cu/Dia-Ga nanofluids concerning the modified Lewis number are investigated. The calculated solutions are validated by trend comparison with previously published results. The following findings can be summarized and concluded as follows:

•The Chebyshev spectral technique greatly and accurately forecasts the existent control of critical thermal stability parameters on the magneto nanofluid behaviour compared with other models and accurately replicates some of the experimental details approximately at 10^{-5};

•The thermo-hydromagnetic stability of the liquid-metal-based (Copper-Gallium nanofluid and Copper/Diamond-Gallium) and the water-based nanofluids (Copper-water) cases. It is computationally discovered that Cu/Dia-Ga nanofluid is 80% more stable than the Cu-Water counterparts;

•The liquid-metal-based magneto nanofluids, Cu/Dia-Ga are more stable and less complex in geometry, particularly the bottom-heavy nanoparticle Distribution;

• Increase in porosity ε and the Darcy number also show an increase in the critical Rayleigh number R_{ac} signifying stability of the system;

• The effect of the increase in the modified magnetic Chandrasekhar number Q with regards to the Darcy number Da shows pull back at the onset of convection for both nanoparticle dispersals;

•The onset of convection is accelerated for the top-heavy dispersals of nanoparticles as the nanoparticle Rayleigh number R_N increases

•The effects of the modified specific heat increment N_B on the Copper-Gallium andCopper/Diamond-Gallium magneto nanofluid is relatively insignificant in the device.

REFERENCES

[1]. Qureshi, A. Z. (2016). Heat and mass transfer analysis of MHD nanofluid flow with radiative heat effects in the presence of spherical Au-Metallic nanoparticles. Nanoscale Research Letters, 11:472.

[2]. Kun-Quan, M., & Jing, L. (2006). Nano Liquid-metal as ultimate coolants. China: Elsevier.

[3]. Chang, N. K. (2014). Liquid metal magnetohydrodynamic flows in an electrically conducting rectangular duct with sudden expansion. Computers & Fluids , 89, 232-241.

[4]. Sakshi, A., & Sunita, S. (2011). Nanofluids: Future Industrial Coolants. AIP (pp. 301-302). Chandigarh: American Institute of Physics.

[5]. Siddiqui, A. A., & Chamkha, A. J. (2020). Thermo-magnetohydrodynamic effects on Cu+engine oil/water nanofluid flow in a porous media-filled annular region bounded by two rotating cylinders. Journal Mechanical Engineering Science, 1-16.

[6]. Nield, D. A., & Bejan, A. (2017). Convection in porous media. Durham: Springer.

[7]. Yadav, D., Bhargava, R., & Agrawal, G. S. (2013). Thermal instability in a nanofluid layer with a vertical magnetic field. Journal of Engineering Mathematics, 147-164.

[8]. Wakif, A., Boulahia, Z., & Sehaqui, R. (2017). Numerical analysis of the onset of longitudinal convective rolls in a porous Medium Saturated by an Electrically Conducting Nanofluid in the Presence of an External Magnetic Field. Results in Physics, 2211-3797.

[9]. Wakif, A., Boulahia, Z., Zaydan, M., Yadil, N., & Sehaqui, R. (2016). The Power Series Method to Solve a Magneto-Convection Problem in a Darcy-Brinkman Porous Medium Saturated by an Electrically Conducting Nanofluid Layer. International Journal of Innovation and Applied Studies, 1048-1065.

[10]. Barletta, A., Schio, E. R., & Storesletten, I. (2013). Convective Instability in a Horizontal Porous Channel with Permeable and Conducting Side Boundaries. Transparent Porous Media, 515-533.